

# Silicon Photonic Integrated Optoelectronic Oscillator for Frequency-Tunable Microwave Generation

Weifeng Zhang, *Member, IEEE*, and Jianping Yao , *Fellow, IEEE, Fellow, OSA*

(Invited Paper)

**Abstract**—Photonic generation of a frequency-tunable microwave signal based on a silicon photonic integrated optoelectronic oscillator (OEO) is proposed and experimentally demonstrated. The silicon photonic chip includes a high-speed phase modulator (PM), a thermally tunable micro-disk resonator (MDR), and a high-speed photodetector (PD). When an external light wave is injected into the chip, by a joint use of the PM, the MDR, and the PD, a bandpass microwave photonic filter (MPF) based on phase modulation and phase-modulation to intensity-modulation (PM-IM) conversion is realized. If the output microwave signal from the MPF is fed to the microwave input port of the PM with a sufficiently large gain provided by an electrical amplifier, the MPF becomes an OEO. By controlling the electrical power applied to a micro-heater, the resonance frequency of the MDR is tuned, which leads to the tuning of the MPF, and thus, the OEO oscillation frequency. In the experimental demonstration, two silicon photonic integrated OEOs using two MDRs with different micro-heaters are studied. The first OEO has a high-resistivity metallic micro-heater placed on top of the MDR, and the second OEO has a p-type doped silicon heater in the MDR. The two thermally tunable MDRs are characterized, and the performance of the MPFs based on the two MDRs is evaluated. The use of the two MPFs to implement two OEOs is performed, and their performance is evaluated in terms of frequency tunable range, phase noise, and power consumption.

**Index Terms**—Microdisk resonator, microwave photonics, optoelectronic oscillator, phase modulator, photodetector, photonic microwave generation, silicon photonics.

## I. INTRODUCTION

TO achieve high-resolution target detection and high speed communications, radar and wireless systems are expected to operate at higher frequencies and broader bandwidths [1], [2]. In response to such a demand, a high-frequency microwave source with a broad frequency tunable range is highly required. Pure electronic oscillators may not be able to generate a microwave signal at such a high frequency while maintaining a low phase noise [3], [4]. To overcome this challenge, photonic

generation of microwave signals has been a topic of interest in the last few years [5]–[12]. The key advantages of using photonics to generate a microwave signal are the high frequency and large frequency tunable range while the phase noise can be maintained low.

Among various photonic generation approaches, microwave generation based on an optoelectronic oscillator (OEO) has been considered an effective solution for the generation of a high frequency and ultra-low phase noise microwave signal [13]–[15]. To ensure an OEO to operate in single mode, a high-selectivity bandpass filter (BPF) must be used. In earlier demonstrations, the high-selectivity bandpass filter is usually an electrical BPF. The use of an electrical BPF has two limitations. First, it is not tunable or with a very limited tunable range, thus a microwave signal with a fixed frequency or a small frequency tunable range can be generated [16], [17]. Second, a high frequency electrical BPF usually has a wide bandwidth. To ensure single frequency operation, the bandwidth must be small, which would limit the highest operating frequency. To overcome these two limitations, we may use a microwave photonic filter (MPF) [18]–[22]. An MPF can have a high center frequency while maintaining a narrow bandwidth. Different OEOs using an MPF are proposed and experimentally demonstrated [23]–[25]. However, most of the reported OEOs are implemented based on discrete optical components, which makes the system bulky, expensive and with high-power consumption. For practical applications, it is highly desirable that an OEO is implemented using a photonic integrated circuit (PIC). With rapid development of silicon photonics, extensive efforts have been directed to the use of silicon photonic technology in the implementation of microwave photonic systems [26], [27], due to its compatibility with current CMOS technology and potential for seamless integration with electronics [28].

Recently, we have reported an integrated MPF on a silicon photonic chip [29]. The chip includes three key components: a high-speed phase modulator (PM), a thermally-tunable high-selectivity micro-disk resonator (MDR), and a high-speed photodetector (PD). When an external optical wave is injected into the chip, by jointly using the PM, the MDR and the PD, a bandpass MPF is realized based on phase modulation and phase-modulation to intensity-modulation (PM-IM) conversion. By amplifying the output signal from the MPF and feeding it back to the input of the MPF, the MPF becomes an integrated OEO. If the gain is higher than the loss, microwaves oscillation will

Manuscript received February 28, 2018; revised April 16, 2018; accepted April 20, 2018. Date of publication April 24, 2018; date of current version August 30, 2018. This work was supported in part by the Natural Science and Engineering Research Council of Canada (NSERC) through the CREATE program and the CMC Microsystems. (Corresponding author: Jianping Yao.)

The authors are with the Microwave Photonics Research Laboratory, School of Electrical Engineering and Computer Science, University of Ottawa, Ottawa, ON K1N 6N5, Canada (e-mail: wzhan088@uottawa.ca; jpyao@eecs.uottawa.ca).

Color versions of one or more of the figures in this paper are available online at <http://ieeexplore.ieee.org>.

Digital Object Identifier 10.1109/JLT.2018.2829823

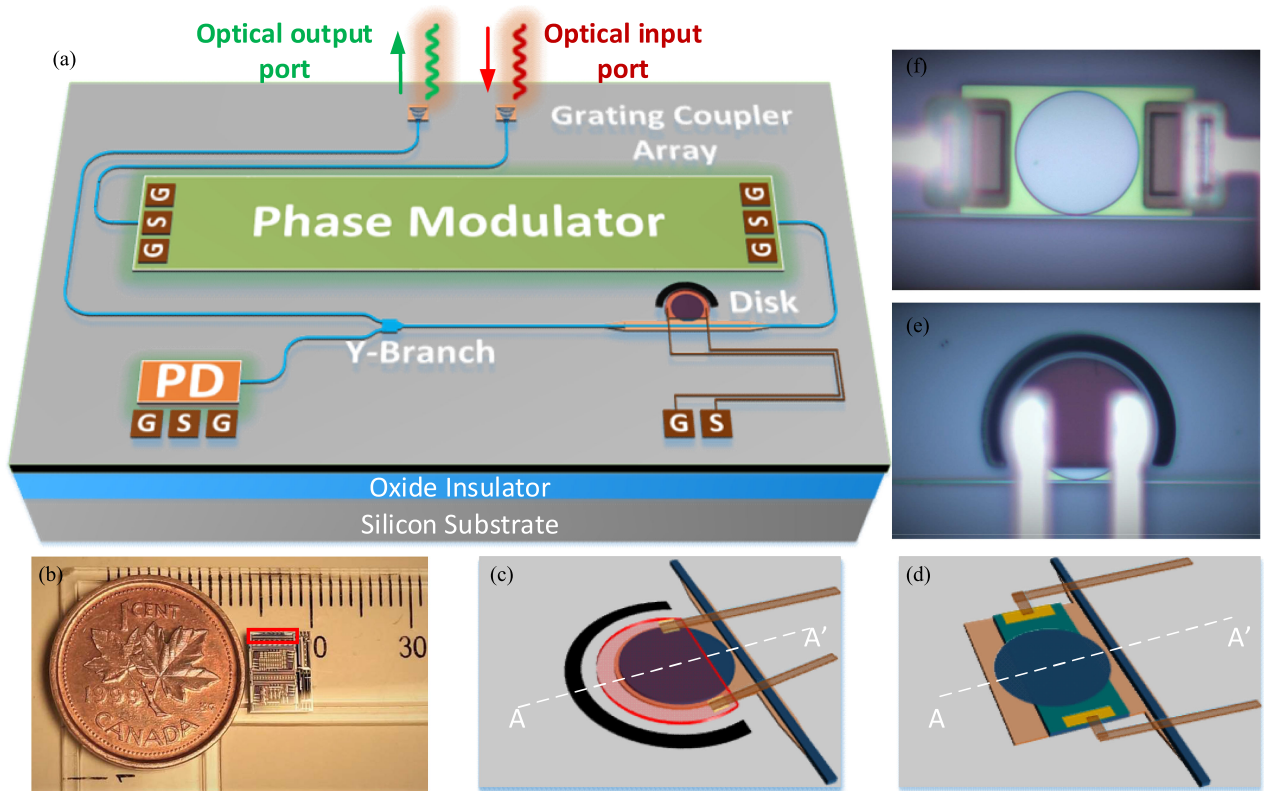


Fig. 1. Schematic of the proposed silicon photonic OEO. (a) Perspective view of the proposed OEO; (b) the fabricated chip prototype captured by a microscope camera; (c) perspective view of the MDR with a top-placed micro-heater; (d) perspective view of the MDR with a p-type doped micro-heater; (e) image of the MDR with a top-placed micro-heater; and (f) image of the MDR with a p-type doped micro-heater.

start and the oscillation frequency is determined by the central frequency of the passband of the MPF [30]. By controlling the electrical power applied to the micro-heater which is located on top of the MDR, the resonance frequency of the resonator is tunable, which leads to the tuning of the central frequency of the passband of the MPF, and thus the frequency of the generated microwave signal from the OEO is tuned.

The work reported in this paper is an extension of our earlier work reported in [30]. Here, a more detailed study, including the frequency tunable range, phase noise and power consumption, is performed. Two OEOs using two MDRs with different micro-heaters are fabricated and demonstrated. In the first OEO, a high-resistivity metallic micro-heater is placed on top of the MDR (MDR1), and in the second OEO, a p-type doped silicon heater is incorporated in the MDR (MDR2). The two thermally-tunable MDRs are firstly characterized, then the performance of the MPFs based on the two MDRs are evaluated. The use of the two MPFs to implement two OEOs are performed. The performance in terms of frequency tuning range, phase noise, and power consumption are evaluated. Both OEOs are able to generate a microwave signal with a frequency tuning range from 3 to 8 GHz. The phase noise of the generated microwave signal for the two OEOs is measured to be around  $-80$  dBc/Hz at a 10-KHz offset frequency. Thanks to the high-level integration, the integrated OEOs have the key advantages in terms of low loss, high stability and large frequency tuning range. This successful demonstration would boost the research on monolithic

integration of the OEOs and the large-scale practical deployment of the OEOs for microwave generation.

## II. OEO DESIGN AND PRINCIPLE

Fig. 1(a) illustrates the schematic of a silicon photonic integrated frequency-tunable OEO. Three key components including a high-speed PM, a thermally-tunable high-selectivity MDR, and a high-speed PD are monolithically integrated on a silicon photonic chip. A grating coupler array with a center-to-center spacing of  $127\ \mu\text{m}$  is used to couple light into and out of the chip, through the use of a fiber array. To reduce the chip footprint, single-mode wire waveguide is mostly employed to guide optical signals in the chip. When an external optical wave is coupled into the chip, the optical wave is firstly routed to the high-speed PM, where a phase-modulated optical signal is generated. Then, the phase-modulated optical signal passes through the high-selectivity MDR, to filter out one sideband. At the output of the MDR, a 3-dB Y-branch coupler is used to split the optical signal equally into two channels. One channel of the optical signal is directly guided to the high-speed PD, where a microwave signal is generated, and the other channel is routed to the output grating coupler to couple the light out of the chip for real-time optical spectrum monitoring.

The chip is fabricated using a CMOS compatible process with 248-nm deep ultraviolet lithography. Fig. 1(b) shows the fabricated silicon photonic chip, in which the red line shows the

area of the OEO ( $4.71 \times 0.64 \text{ mm}^2$ ). In order to improve the selectivity, the MDR is specifically designed to have an additional slab waveguide to wrap the disk and the bus waveguide to reduce the waveguide sidewall scattering loss caused by sidewall roughness. Thanks to the slab waveguide, part of the disk sidewall is made away from the confined optical mode, which would weaken the impact of the sidewall roughness on the optical field, to reduce the loss and thus increase the Q-factor of the MDR [31]. By using the thermal-optic effect, the MDR could be thermally tunable. In the implementation, two MDRs with two different micro-heaters are used. Fig. 1(c) and (d) shows the perspective views of the two MDRs with different micro-heaters. In Fig. 1(c), the MDR has a high-resistivity metallic micro-heater placed on top of the disk; in Fig. 1(d), the MDR has a p-type doped silicon heater in the disk. The heavy p-type implantation creates a doped resistor for efficient thermal tuning of the MDR. Fig. 1(e) and (f) are the images of the two fabricated MDRs captured by a microscope camera.

In our demonstration, an OEO is realized by incorporating an MPF implemented based on phase modulation and PM-IM conversion. When an external optical wave is coupled into the chip, a phase-modulated optical signal is generated at the output of the PM and is sent to the high-selectivity MDR, which serves as an optical notch filter. If the phase-modulated optical signal is directly applied to a PD, no microwave signal will be recovered due to the out of phase nature between the two first-order sidebands of a phase-modulated optical signal. If one of the two sidebands of the phase-modulated optical signal is attenuated by locating it in the notch of the MDR, the phase-modulated signal is converted to an intensity-modulated single-sideband signal, and a microwave signal is generated at the PD. The entire operation corresponds to a bandpass MPF, of which the spectral response of the microwave filter is directly translated from the spectral response of the MDR. Thanks to the ultra-narrow notch and thermal tunability of the MDR, the MPF has a narrow passband and is tunable. By feeding the microwave signal at the output of the MPF to its input and providing a sufficiently large gain using an electrical power amplifier, the MPF becomes an OEO. By tuning the notch of the MDR, the center frequency of the MPF filter is tuned, and thus the frequency of the generated microwave signal is tuned.

### III. EXPERIMENT

Two MDRs with two different micro-heaters are used in the experimental demonstration. In the experiment, to control and stabilize the chip temperature, a thermoelectric-cooler (TEC) is used. The silicon chip is placed on the TEC, and a thermistor is placed adjacent to the chip, to measure and provide a feedback temperature to a commercial TEC controller. During the experiment, the chip temperature is stabilized at  $23 \text{ }^\circ\text{C}$ .

#### A. High-Speed PM

Thanks to the free-carrier plasma dispersion effect in silicon, a high-speed PM on silicon could be achieved. In our designs, a traveling wave structure is used, where a lateral pn junction is incorporated in the rib waveguide to achieve high-speed

modulation. When the reverse bias voltage is 4 V, the 3-dB modulation bandwidth is measured to be 20.85 GHz.

#### B. Tunable MDRs

As a key component in the chip, an MDR plays a critical role in determining the spectral response of the MPF. A higher Q-factor of a MDR, a higher selectivity of the MPF. To elevate the selectivity and strengthen the optical coupling between the disk and the bus waveguides, an additional slab waveguide is used to wrap the disk and the bus waveguide to weaken the impact of the disk sidewall roughness on the optical field confinement [31]. In the design, the two MDRs are designed to have an all-pass configuration, both having a radius of  $10 \text{ }\mu\text{m}$  and a height of 220 nm, and the bus waveguides have a height of 220 nm. The additional slab waveguide has a height of 90 nm. To simplify the design, the widths of the slab waveguide around the disk and the bus waveguide are kept identical of 200 nm, and in the coupling region the two slab waveguides are designed to fully overlap. To effectively excite the first-order whispering-gallery-mode (WGM), the width of the bus waveguide is controlled to be 600 nm.

For both MDRs, the thermal-optic effect is used to perform wavelength tuning. In the two MDRs, two different micro-heaters are used. Fig. 2(a) shows a cross-sectional view of the first MDR (MDR1) with a top-placed micro-heater along the white dashed line AA' in Fig. 1(c). A high-resistivity metallic micro-heater is placed on top of the disk. To avoid the thermal impact on neighboring components in the chip, a deep trench is etched around the disk for thermal isolation. Fig. 2(b) shows the measured transmission spectrum of MDR1 using an optical vector analyzer (OVA, LUNA OVA CTe). First-order and second-order WGMs are effectively excited in the disk. The first-order WGM is measured to have a free spectral range (FSR) of 10.7 nm, and the second-order WGM has an FSR of 10.6 nm. Fig. 2(c) gives the measured resonance WGM<sub>2,103</sub> at a wavelength of 1542.38 nm and its Lorentzian fitting. The notch has a 3-dB bandwidth of 14 pm, corresponding to a Q-factor of around  $1.10 \times 10^5$ , and an extinction ratio of 4 dB. Fig. 2(d) shows the spectrum tuning of the MDR when the applied electrical power to the micro-heater is increased. The color indicates the measured optical power, and the red dashed line shows the resonance frequency of the WGM<sub>2,104</sub> with different applied electrical power. Due to the thermal-optic effect, the refractive index of the silicon is increased with the increase in temperature, which leads to a red-shift of the MDR transmission spectrum. The resistance of the micro-heater is calculated to be 27.1  $\Omega$ . When the applied electrical power to the micro-heater is 110.4 mW, the red-shift amount of the transmission spectrum is one FSR. The wavelength shift rate is calculated to be 96 pm/mW.

Fig. 2(e) shows a cross-sectional view of the second MDR (MDR2) with a p-type doped silicon heater along the white dashed line AA' in Fig. 1(d). The heavy p-type implantation creates a doped resistor in the disk. Fig. 2(f) shows the measured transmission spectrum of the MDR using the same OVA. First-order, second-order and third-order WGMs are effectively excited in the disk. The first-order WGM is measured to have an

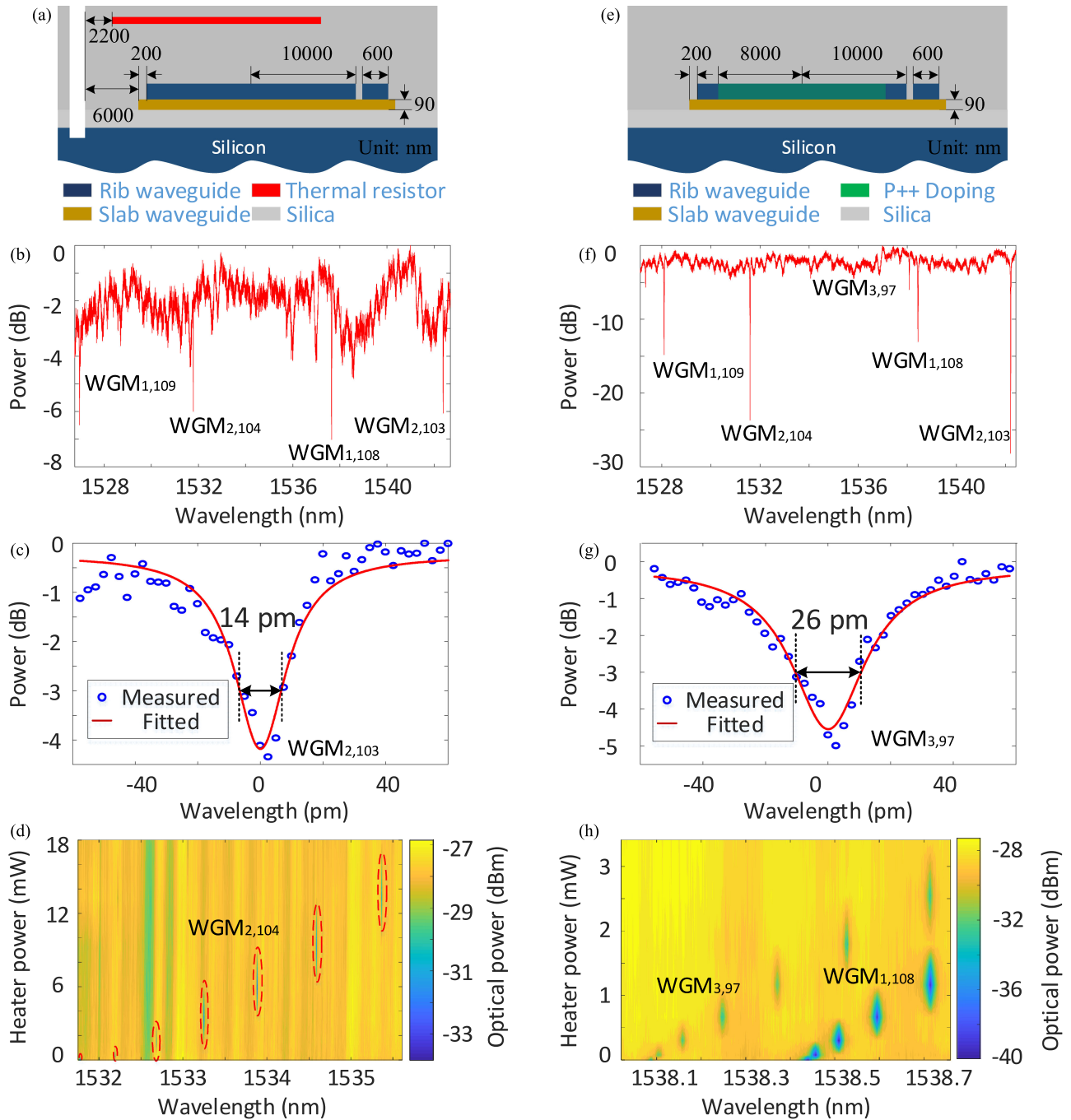


Fig. 2. (a) Cross-sectional view of the MDR with a top-placed micro-heater; (b) measured transmission spectrum; (c) zoom-in view of the WGM<sub>2,103</sub>; (d) spectrum tuning of the MDR with a voltage applied to the micro-heater; (e) cross-sectional view of the MDR with a p-type doped micro-heater; (f) measured transmission spectrum; (g) zoom-in view of the WGM<sub>3,97</sub>; and (h) spectrum tuning of the MDR with a voltage applied to the micro-heater.

FSR of 10.3 nm, the second-order WGM has an FSR of 10.6 nm, and the third-order WGM has an FSR of 10.7 nm. Fig. 2(g) gives the measured resonance WGM<sub>3,97</sub> at a wavelength of 1538.09 nm and its Lorentzian fitting. The notch has a 3-dB bandwidth of 26 pm, corresponding to a Q-factor of around  $0.6 \times 10^5$ , and an extinction ratio of 4.5 dB. The smaller Q-factor is due to the large optical absorption loss induced by the heavy doped implantation. Fig. 2(h) shows the spectrum tuning of the MDR when the applied electrical power to the micro-heater is increased. The resistance of the micro-heater is calculated to be 330  $\Omega$ . When

the applied electrical power to the micro-heater is 13.2 mW, the red-shift amount of the transmission spectrum is 3.3 nm. The wavelength shifting rate is calculated to be 250 pm/mW.

The difference shown in the transmission spectra of the two MDRs is due to the different index perturbations induced by the metallic and doped micro-heaters in the MDRs. Since the doped resistor would introduce an additional optical absorption loss, its Q-factor is smaller than the one with the top-placed metallic micro-heater. In the meanwhile, the MDR with a doped micro-heater has a higher wavelength shifting rate than the one

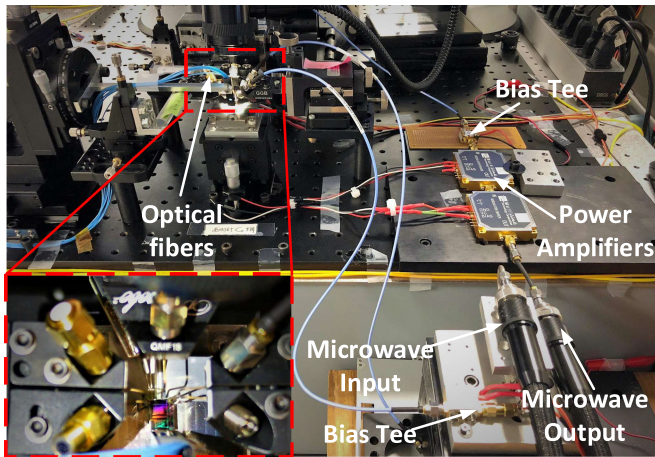


Fig. 3. Experimental setup. The fiber array and electrical probes connected to the chip are shown in an enlarged red-dashed box.

with a top-placed micro-heater. Since a higher Q-factor is more important, especially for the implementation of an OEO where a higher selectivity of the MPF is needed, the MDR with a top-placed micro-heater is a better choice in the design and implementation of an integrated OEO.

### C. High-Speed PD

A high-speed silicon photonic PD can be implemented based on germanium doping. For both designs, an identical germanium-on-silicon pin PD is implemented. At a reverse bias voltage of 7.5 V, the PD has a 3-dB bandwidth of 15.69 GHz.

### D. Frequency-Tunable MPFs

The operation and the performance of the MPFs based on the two MDRs are evaluated. Fig. 3 shows the image of the experimental set-up. Thanks to the high-level integration of the chip, the set-up is simple and only an external laser source is required, which makes the system to have a stable operation and low power consumption. The inset shows the electrical probes connected to the PM, the MDR and the PD. A CW light generated by a tunable laser source (Anritsu MG9638A) is sent to the chip via a polarization controller (PC) which is used to adjust the state of polarization (SOP) of the input light to the chip to minimize the polarization-dependent loss. A vector network analyzer (VNA, Keysight N5227A) is used to measure the frequency response. An incoming microwave signal from the VNA is tuned from 2 to 10 GHz with a constant power of 10 dBm. A microwave probe with a GSG configuration in combination with a bias tee is connected to the microwave port of the PM to apply the microwave signal together with a reverse bias voltage to the PM. At the end of the PM, a matched impedance terminator is used to minimize the microwave signal reflection. The phase-modulated signal is sent to an MDR, with one of the sideband being filtered out by the notch of the MDR. To tune the MDR, a DC voltage is applied to the micro-heater to generate the heat. By using a PD, the optical signal is converted to a microwave signal. To collect the microwave signal, another microwave probe with a GSG configuration in combination with a bias tee is connected

to the output of the PD. At the optical output coupler, an optical spectrum analyzer (OSA) is connected to real-time monitor the optical spectrum of the optical signal from the MDR. Three high-precision voltage source meters (Keithley 2400) are used to provide the bias voltages for the PM, the MDR, and the PD.

For the chip with a top-placed micro-heater, the PM is reverse biased at 3.6 V and the PD is reverse biased at 8.8 V. The bias voltage for MDR1 is tuned from 0 to 0.13 V to tune the filter frequency response. Fig. 4(a) shows the measured frequency response of the MPF with a center frequency tuned from 2 to 10 GHz when the applied electrical power to the micro-heater of the MDR varies from 0 to 0.6 mW, in which the color indicates the normalized power of microwave signal. As can be seen, a frequency tuning range as broad as 8 GHz is achieved with a power consumption as small as 0.6 mW, which demonstrates the key advantage of an integrated MPF in the terms of a broad frequency tuning and low power consumption. Note that the peak power of the frequency response is becoming smaller with the increase of the center frequency, which is caused by the limited bandwidths of the PM and PD. Fig. 4(b) shows the filter frequency response with a center frequency of 5.0 GHz when the applied electrical power to the micro-heater is 0.2 mW. The MPF is measured to have a 3-dB bandwidth of 1.8 GHz, which matches well with the 3-dB bandwidth of the notch of the MDR, and an extinction ratio of 19.6 dB.

For the chip with a p-type doped silicon heater, the PM is reverse biased at 3.5 V and the PD is reverse biased at 8.6 V. The bias voltage for the MDR is tuned from 1.08 to 1.28 V to tune the filter frequency response. Fig. 4(c) shows the measured frequency response of the MPF with a center frequency tuned from 2 to 10 GHz when the applied electrical power to the micro-heater of the MDR varies from 0.36 to 0.50 mW. As can be seen, a frequency tuning range as broad as 8 GHz is achieved with a power consumption as small as 0.50 mW, which again demonstrates the key advantage of the integrated MPF in the terms of a broad frequency tuning and low power consumption. Fig. 4(d) shows the filter frequency response with a center frequency of 4.8 GHz when the applied electrical power to the micro-heater is 0.43 mW. This MPF is measured to have a 3-dB bandwidth of 2.7 GHz, which matches well with the 3-dB bandwidth of the notch of the MDR, and an extinction ratio of 7.1 dB.

The frequency response difference between the two MPFs shown in Fig. 4 is due to the different notch profiles of the MDRs. The metallic and doped micro-heaters impose a different index perturbation on the disks and optical coupling, which leads to the notch difference of the MDRs. Especially, the p-type doped heater introduces a large optical absorption loss, which cause a wider bandwidth and poorer selectivity of the MPF.

### E. Frequency-Tunable OEOs

By feeding the output signal from the PD to the microwave input port of the PM through an electrical amplifier with a gain larger than the loop loss, the MPF becomes an OEO and microwave oscillation starts. The oscillation frequency of the OEO could be tuned by tuning the center frequency of the

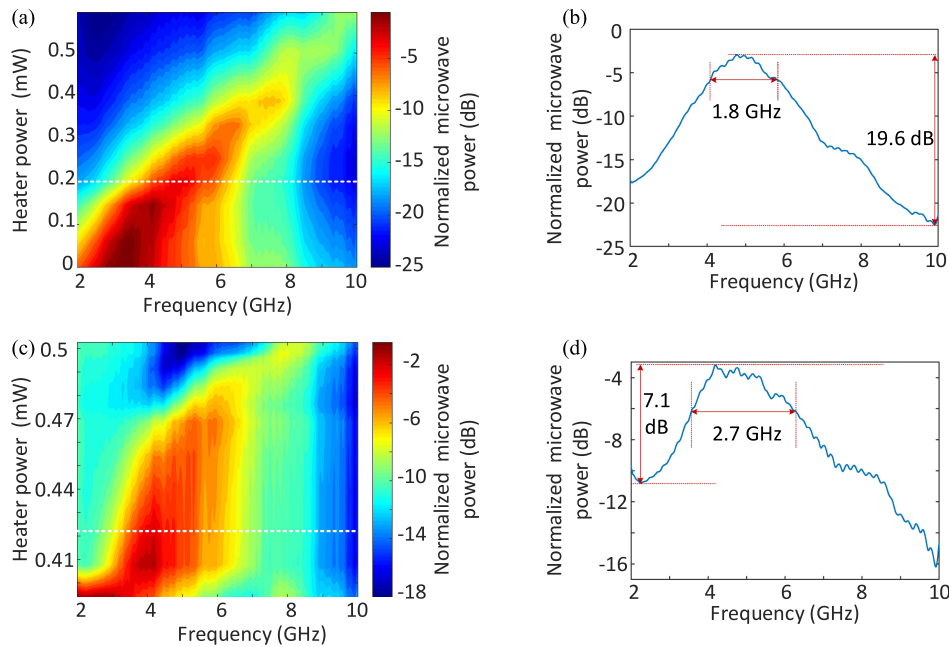


Fig. 4. Experimental results of the MPFs. (a) Measured frequency responses of the MPF with a top-placed micro-heater; (b) frequency response of the MPF with a center frequency of 5.0 GHz; (c) measured frequency responses of the MPF with a p-type doped silicon heater; and (d) frequency response of the MPF with a center frequency of 4.8 GHz.

MPF via applying a different bias voltage to the micro-heater of the MDR. In the OEO experiment, the output signal from the PD is equally divided by an electrical coupler into two paths. In one path, the signal is amplified by two cascaded power amplifiers (MultiLink modulator driver MTC5515-751) and fed to the microwave input of the PM; in the other path, the microwave signal is guided to an electrical spectrum analyzer (ESA, Agilent E4448A) for real-time spectrum monitoring and a signal source analyzer (SSA, Agilent E5052B) for phase noise measurements.

For the chip with a top-placed micro-heater, Fig. 5(a) shows the measured electrical spectrum of the generated microwave signal at 4.74 GHz, where the frequency span is 6 GHz and the resolution bandwidth (RBW) is 200 KHz. A side-mode suppression ratio (SMSR) as high as 67 dB is observed. Fig. 5(b) shows the electrical spectrum of the generated 4.74-GHz signal with a frequency span of 25 GHz and a RBW of 200 KHz. As can be seen, higher-order harmonics are observed, which are caused by the nonlinearity in the OEO loop. Fig. 5(c) shows the measured optical spectrum at the output grating coupler of the chip when the OEO is operating at 4.74 GHz. It is clear to see that the power of the upper first-order sideband is smaller than that of the lower first-order sideband by 4 dB. The sideband suppression ratio could be improved if an MDR operating in the critical coupling condition is employed by re-designing the coupling gap and length. Although the upper sideband is not completely removed, the residual power is very small, and an effective PM-IM conversion is achieved. Fig. 5(d) shows the measured phase noise of the generated microwave signal when the OEO is operating at 4.74 GHz. The phase noise at a 10-KHz offset frequency is measured to be  $-81$  dBc/Hz, which is large considering the loop length is very small. The phase noise performance can be

further improved by adding an optical waveguide delay line in the chip to increase the loop length or by using an MDR with a higher Q-factor.

The frequency tunability of the OEO is also investigated. By tuning the bias voltage to the micro-heater, the notch of the MDR is shifted and thus the frequency of the generated microwave signal is tuned. Fig. 5(e) shows the superimposed spectrums of the generated microwave signal with its frequency tuned from 3 to 7.4 GHz. As can be seen, with the frequency of the generated microwave signal tuned, a high SMSR is still maintained. Since the MPF has a lower gain at a higher frequency and the two microwave amplifiers could not offer an enough gain to support the OEO to operate at a frequency higher than 7.4 GHz, the frequency tunable range is limited to 3 to 7.4 GHz in this experimental demonstration. Fig. 5(f) shows the measured phase noise of the generated microwave signal when its frequency is tuned. It is clear to see the phase noise of the generated microwave signal maintains around  $-80$  dBc/Hz at the offset frequency of 10 KHz, which verifies the key advantage of an OEO to have a constant phase noise with the increase in oscillation frequency.

For the chip with a p-type doped micro-heater, Fig. 6(a) shows the measured electrical spectrum of the generated microwave signal at 4.56 GHz, where the frequency span is 6 GHz and the RBW is 200 KHz. An SMSR as high as 61 dB is observed. Fig. 6(b) shows the electrical spectrum of the generated 4.56-GHz signal with a frequency span of 25 GHz and a RBW of 200 KHz. Again, higher-order harmonics are observed, which are caused by the nonlinearity in the OEO loop. Fig. 6(c) shows the measured optical spectrum at the output grating coupler of the chip when the OEO is operating at 4.56 GHz. It is clear to see that the power of the upper first-order sideband is smaller than that of the lower first-order sideband by 7 dB, which again verifies

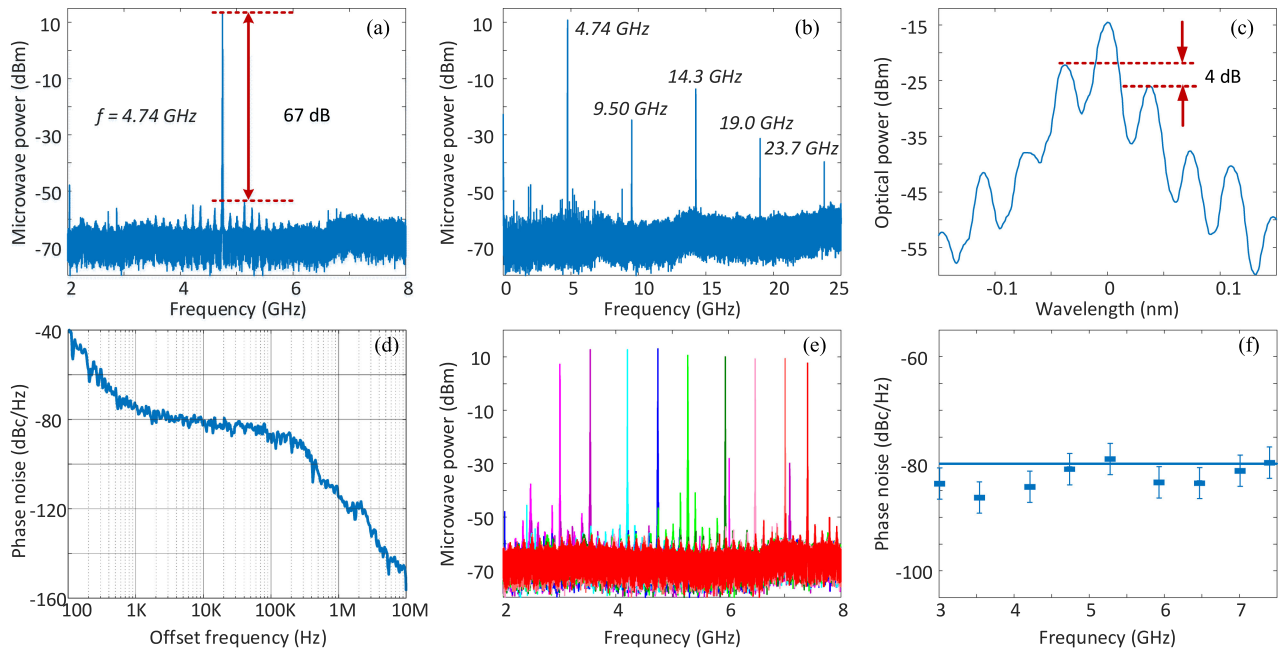


Fig. 5. Experimental result of the OEO with a top-placed micro-heater. (a) Electrical spectrum of the generated 4.74 GHz signal with a frequency span of 6 GHz and a RBW of 200 KHz; (b) electrical spectrum of the generated 4.74 GHz signal with a frequency span of 25 GHz and a RBW of 200 KHz; (c) measured optical spectrum at the optical output grating coupler when the OEO is operating at 4.74 GHz; (d) measured phase noise of the generated microwave signal when the OEO is operating at 4.74 GHz; (e) measured electrical spectrums of the generated microwave signal at different frequencies. The frequency is coarsely tuned from 2 to 8 GHz and the RBW is 200 KHz; and (f) measured phase noise of the generated microwave signal at different frequencies.

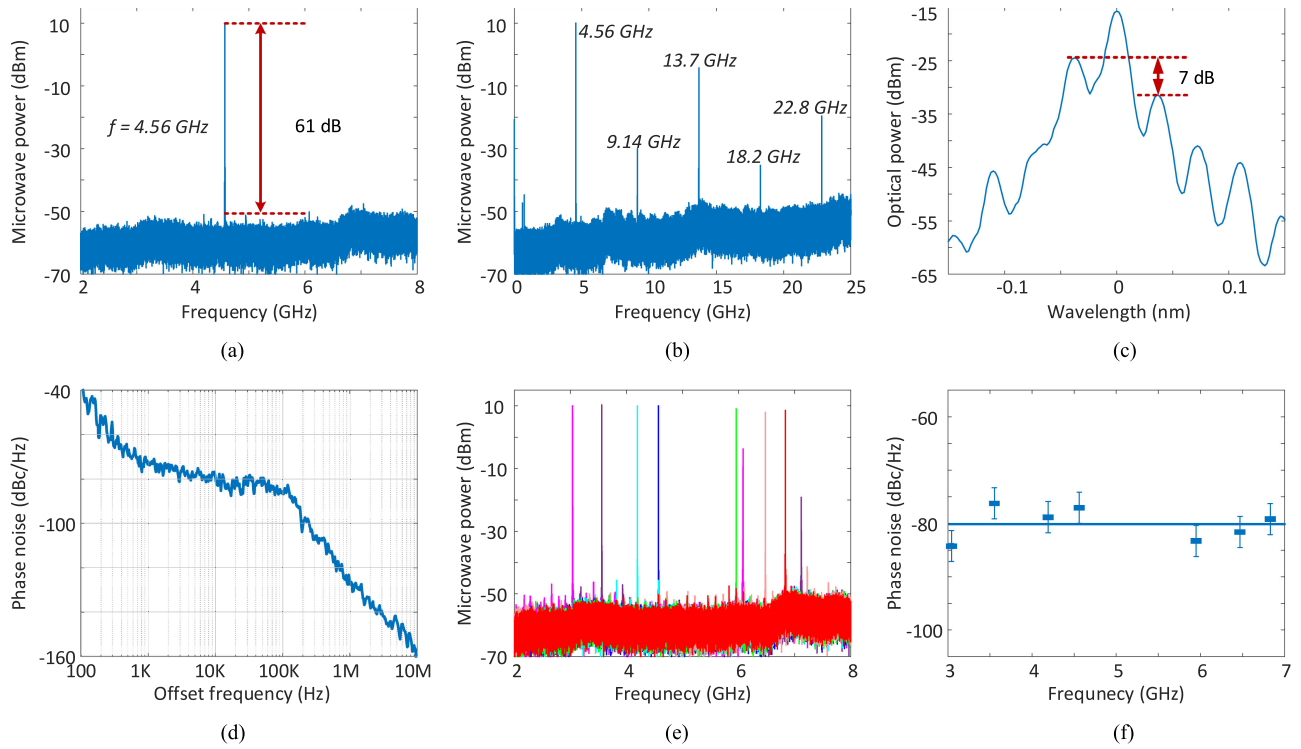


Fig. 6. Experimental result of the OEO with a p-type doped silicon heater. (a) Electrical spectrum of the generated 4.56 GHz signal with a frequency span of 6 GHz and a RBW of 200 KHz; (b) electrical spectrum of the generated 4.56 GHz signal with a frequency span of 25 GHz and a RBW of 200 KHz; (c) measured optical spectrum at the optical output grating coupler when the OEO is operating at 4.56 GHz; (d) measured phase noise of the generated microwave signal when the OEO is operating at 4.56 GHz; (e) measured electrical spectrums of the generated microwave signal at different frequencies. The frequency is coarsely tuned from 2 to 8 GHz and the RBW is 200 KHz; and (f) measured phase noise of the generated microwave signal at the different frequencies.

TABLE I  
HEATER POWER CONSUMPTION OF OEOs FOR FREQUENCY TUNING

OEO	Frequency (GHz)	DC Voltage (V)/ Current (mA)	Power (mW)
OEO with a top- placed heater	3.1	0.01/0.33	0.003
	3.5	0.02/0.71	0.014
	4.2	0.03/1.10	0.033
	4.7	0.05/1.82	0.091
	5.3	0.07/2.69	0.188
	5.9	0.08/3.06	0.245
	6.5	0.09/3.36	0.302
	7.4	0.11/3.81	0.419
OEO with a p-type doped silicon heater	3.0	1.09/0.33	0.360
	3.6	1.14/0.34	0.388
	4.2	1.16/0.35	0.406
	4.6	1.18/0.36	0.425
	6.0	1.22/0.38	0.464
	6.5	1.25/0.39	0.488
	6.9	1.28/0.39	0.499

that an effective PM-IM conversion is achieved. Fig. 6(d) shows the measured phase noise of the generated microwave signal when the OEO is operating at 4.56 GHz. The phase noise at a 10-KHz offset frequency is measured to be  $-78$  dBc/Hz, which is also large considering the loop length is very small. The low phase noise is due to the high Q-factor of the MDR.

The frequency tunability of the OEO is also investigated. Fig. 6(e) shows the superimposed spectrums of the generated microwave signal with its frequency tuned from 3 to 6.8 GHz. As can be seen, with the frequency of the generated microwave signal tuned, a high SMSR is still maintained. In addition, near the frequency of 5 GHz, there is no microwave oscillation. This is because the filter selectivity is undermined since the doped silicon heater induces a large optical absorption loss at this point, which inhibits the single mode oscillation in the OEO loop. Fig. 6(f) shows the measured phase noise of the generated microwave signal when its frequency is tuned. It is clear to see the phase noise of the generated microwave signal maintains around  $-80$  dBc/Hz at the offset frequency of 10 KHz, which verifies again the key advantage of an OEO to have a constant phase noise with the increase in oscillation frequency.

The power consumption of the two OEOs is also evaluated. Table I summarizes the power consumption of the two OEOs when operating at different frequencies. Overall, the OEOs have a low power consumption, which is attributed to the low power needed for thermal tuning of the MDRs. Specifically, with a frequency tuning range from 3 to 7.4 GHz, the OEO with a top-placed micro-heater has a power consumption from 0.003 to 0.419 mW, a net power consumption increase of 0.416 mW. The frequency shifting rate is calculated to be 10.6 GHz/mW. With a frequency tuning range from 3 to 6.8 GHz, the OEO with a doped micro-heater has a power consumption from 0.360 to 0.499 mW, a net power consumption increase as small as 0.139 mW. The frequency shifting rate is calculated to be 23.7 GHz/mW. The doped micro-heater performs better in terms of frequency shifting rate.

Compared the performance of the two OEOs using two different micro-heaters, the one with a top-placed micro-heater

has better performance in terms of frequency tuning range and phase noise. Since the doped silicon heater induces an optical absorption loss to the MDR, the Q-factor of the MDR is lower and the selectivity of the MPF is poorer, thus the phase noise performance is degraded. For the implementation of an OEO, a high Q-factor is more important, thus an OEO using a top-placed micro-heater is a better choice.

#### IV. CONCLUSION

Silicon photonic integrated OEOs for tunable microwave signal generation have been demonstrated. The key component in a silicon photonic integrated OEO is the MDR, which was designed by adding a slab waveguide to wrap the disk and the bus waveguide to reduce the impact of the sidewall roughness on the optical field confinement. Thus, the loss of the MDR was reduced and the Q-factor was increased. A wideband PM and high-speed PD were also implemented on a single chip. Thus, the overall size of an integrated OEO was small and the power consumption was low. The frequency tuning was achieved by thermally tuning the MDR. In the study, two different micro-heater approaches were employed. Both can provide a frequency tuning range of 8 GHz. Compared with the microwave signal generation of the two OEOs, the OEO with a top-placed micro-heater has a slightly better performance in terms of frequency tuning range and phase noise. Although an OEO based on a p-type doped silicon heater can have a wide tunable range, the optical absorption loss due to the doping is higher, which makes the selectivity of the MPF poorer and the phase noise higher.

To achieve monolithic integration, a laser source must be also integrated into the chip, which can be realized using heterogeneous integration [32]. In addition, thanks to the compatibility of silicon photonic technology with the mature CMOS technology, it is feasible to realize seamless integration between photonic components and electronic circuits to include a bias tee, a microwave power amplifier and a feedback circuit into the chip. Thus, true monolithic integration can be realized and the OEO performance could be significantly improved, making large-scale deployment of on-chip OEOs for applications in microwave systems possible.

#### ACKNOWLEDGMENT

The authors would like to thank CMC Microsystems for providing the design tools and enabling the fabrication of the device.

#### REFERENCES

- [1] D. K. Barton, *Radar System Analysis and Modeling*. Boston, MA, USA: Artech House, 2005.
- [2] A. W. Rihaczek, *Principles of High-Resolution Radar*. Norwood, MA, USA: Artech House, 1996.
- [3] H. D. Griffiths and W. J. Bradford, "Digital generation of high time bandwidth product linear FM waveforms for radar altimeters," *IEE Proc. Radar Signal Process.*, vol. 139, no. 2, pp. 160–169, Apr. 1992.
- [4] H. Kwon and B. Kang, "Linear frequency modulation of voltage-controlled oscillator using delay-line feedback," *IEEE Microw. Wireless Compon. Lett.*, vol. 15, no. 6, pp. 431–433, Jun. 2005.
- [5] J. Capmany and D. Novak, "Microwave photonics combines two worlds," *Nature Photon.*, vol. 1, no. 6, pp. 319–330, Apr. 2007.
- [6] R. Won, "Microwave photonics shines," *Nature Photon.*, vol. 5, no. 12, Dec. 2011, Art. no. 736.

- [7] J. P. Yao, "Microwave photonics," *J. Lightw. Technol.*, vol. 27, no. 3, pp. 314–335, Feb. 2009.
- [8] A. J. Seeds and K. J. Williams, "Microwave photonics," *J. Lightw. Technol.*, vol. 24, no. 12, pp. 4628–4641, Dec. 2006.
- [9] M. Khan *et al.*, "Ultrabroad-bandwidth arbitrary radiofrequency waveform generation with a silicon photonic chip-based spectral shaper," *Nature Photon.*, vol. 4, no. 2, pp. 117–122, Feb. 2010.
- [10] T. M. Fortier *et al.*, "Generation of ultrastable microwaves via optical frequency division," *Nature Photon.*, vol. 5, no. 7, pp. 425–429, Jul. 2011.
- [11] J. Wang *et al.*, "Reconfigurable radio-frequency arbitrary waveforms synthesized in a silicon photonic chip," *Nature Commun.*, vol. 6, Jan. 2015, Art. no. 5957.
- [12] X. Xie *et al.*, "Photonic microwave signals with zeptosecond-level absolute timing noise," *Nature Photon.*, vol. 11, no. 1, pp. 44–47, Jan. 2017.
- [13] X. S. Yao and L. Maleki, "Optoelectronic microwave oscillator," *J. Opt. Soc. Amer. B*, vol. 13, no. 8, pp. 1725–1735, Aug. 1996.
- [14] T. Berceci and P. Herczfeld, "Microwave photonics-A historical perspective," *IEEE Trans Microw. Theory Techn.*, vol. 58, no. 11, pp. 2992–3000, Nov. 2010.
- [15] X. S. Yao and L. Maleki, "Opto-electronic oscillator and its applications," in *Proc. Microw. Photon.*, Technical Dig., Dec. 1996, pp. 265–268.
- [16] S. Poinsot, H. Porte, J. Goedgebuer, W. T. Rhodes, and B. Boussert, "Continuous radio-frequency tuning of an optoelectronic oscillator with dispersive feedback," *Opt. Lett.*, vol. 27, no. 15, pp. 1300–1302, Aug. 2002.
- [17] E. Shumakher, S. Ó. Dúill, and G. Eisenstein, "Optoelectronic oscillator tunable by an SOA based slow light element," *J. Lightw. Technol.*, vol. 27, no. 18, pp. 4063–4068, Sep. 2009.
- [18] J. P. Yao, "A fresh look at microwave photonics filters," *IEEE Microw. Mag.*, vol. 16, no. 8, pp. 46–60, Sep. 2015.
- [19] D. Marpaung *et al.*, "Low-power, chip-based stimulated Brillouin scattering microwave photonic filter with ultrahigh selectivity," *Optica*, vol. 2, no. 2, pp. 76–83, Jan. 2015.
- [20] V. R. Supradeepa *et al.*, "Comb-based radiofrequency photonic filters with rapid tunability and high selectivity," *Nature Photon.*, vol. 6, no. 3, pp. 186–194, Mar. 2012.
- [21] X. Yi and R. A. Minasian, "Microwave photonic filter with single bandpass response," *Electron. Lett.*, vol. 45, no. 7, pp. 362–363, Mar. 2009.
- [22] J. Chou, Y. Han, and B. Jalali, "Adaptive RF-photonic arbitrary waveform generator," *IEEE Photon. Technol. Lett.*, vol. 15, no. 4, pp. 581–583, Apr. 2003.
- [23] S. Pan and J. P. Yao, "Wideband and frequency-tunable microwave generation using an optoelectronic oscillator incorporating a Fabry–Perot laser diode with external optical injection," *Opt. Lett.*, vol. 35, no. 11, pp. 1911–1913, Jun. 2010.
- [24] W. Li and J. P. Yao, "An optically tunable optoelectronic oscillator," *J. Lightw. Technol.*, vol. 28, no. 18, pp. 2640–2645, Sep. 2010.
- [25] W. Li and J. P. Yao, "A wideband frequency-tunable optoelectronic oscillator incorporating a tunable microwave-photonic filter based on phase-modulation to intensity-modulation conversion using a phase-shifted fiber Bragg grating," *IEEE Trans. Microw. Theory Techn.*, vol. 60, no. 6, pp. 1735–1742, Jun. 2012.
- [26] D. Marpaung *et al.*, "Integrated microwave photonics," *Lasers Photon. Rev.*, vol. 7, no. 4, pp. 506–538, Jul. 2013.
- [27] W. Zhang and J. P. Yao, "Silicon-based integrated microwave photonics," *IEEE J. Quantum Electron.*, vol. 52, no. 1, Jan. 2016, Art. no. 0600412.
- [28] B. Jalali and S. Fathpour, "Silicon photonics," *J. Lightw. Technol.*, vol. 24, no. 12, pp. 4600–4615, Dec. 2006.
- [29] W. Zhang and J. P. Yao, "A silicon photonic integrated frequency-tunable microwave photonic bandpass filter," in *Proc. Int. Topical Meeting Microw. Photon.*, Beijing, China, Oct. 2017, pp. 1–4.
- [30] W. Zhang and J. P. Yao, "A silicon photonic integrated frequency-tunable optoelectronic oscillator," in *Proc. Int. Topical Meeting Microw. Photon.*, Beijing, China, Oct. 2017, pp. 1–4.
- [31] W. Zhang and J. P. Yao, "Silicon-based single-mode on-chip ultra-compact microdisk resonator," *J. Lightw. Technol.*, vol. 35, no. 20, pp. 4418–4424, Oct. 2017.
- [32] D. Liang and J. E. Bowers, "Recent progress in lasers on silicon," *Nat. Photon.*, vol. 4, no. 8, pp. 511–517, Aug. 2010.

**Weifeng Zhang** (S'12–M'18) received the B.Eng. degree in electronic science and technology from Xi'an Jiaotong University, Xi'an, China, in 2008, the M.A.Sc. degree in electrical engineering from the Politecnico di Torino, Torino, Italy, in 2011, and the Ph.D. degree in electrical engineering from the University of Ottawa, Ottawa, ON, Canada, in 2017. He is currently a Postdoctoral Fellow in the Microwave Photonics Research Laboratory, School of Electrical Engineering and Computer Science, University of Ottawa.

His current research interests include silicon photonics and its applications in microwave photonics.

**Jianping Yao** (M'99–SM'01–F'12) received the Ph.D. degree in electrical engineering from the Université de Toulon et du Var, France, in December 1997. He is a Distinguished University Professor and University Research Chair in the School of Electrical Engineering and Computer Science, University of Ottawa, Ottawa, ON, Canada. From 1998 to 2001, he was with the School of Electrical and Electronic Engineering, Nanyang Technological University (NTU), Singapore, as an Assistant Professor. In December 2001, he joined the School of Electrical Engineering and Computer Science, University of Ottawa, as an Assistant Professor, where he was promoted to Associate Professor in May 2003 and Full Professor in May 2006. He was appointed the University Research Chair in Microwave Photonics in 2007. In June 2016, he was conferred the title of Distinguished University Professor of the University of Ottawa. From July 2007 to June 2010 and July 2013 to June 2016, he served as Director of the Ottawa-Carleton Institute for Electrical and Computer Engineering. He currently serves as the Chair of the IEEE Photonics Ottawa Chapter, and he is the Technical Committee Chair of IEEE MTT-3 Microwave Photonics. He has authored or coauthored more than 560 research papers including more than 330 papers in peer-reviewed journals and more than 230 papers in conference proceedings.

Prof. Yao is Editor-in-Chief of the IEEE PHOTONICS TECHNOLOGY LETTERS, a Topical Editor of *Optics Letters*, an Associate Editor of *Science Bulletin*, a Steering Committee Member of the IEEE JOURNAL OF LIGHTWAVE TECHNOLOGY, and an Advisory Editorial Board member of *Optics Communications*. He was as a Guest Editor of a Focus Issue on Microwave Photonics in the *Optics Express* in 2013, a Lead-Editor of a Feature Issue on Microwave Photonics in *Photonics Research* in 2014, and a Guest Editor of a special issue on Microwave Photonics in the IEEE JOURNAL OF LIGHTWAVE TECHNOLOGY in 2018. He was a Member of the European Research Council Consolidator Grant Panel in 2016, the Qualitative Evaluation Panel in 2017, and a Member of the National Science Foundation Career Awards Panel in 2016. He has also served as a Chair of a number of international conferences, symposia, and workshops, including the Vice Technical Program Committee (TPC) Chair of the 2007 IEEE Topical Meeting on Microwave Photonics, TPC Co-Chair of the 2009 and 2010 Asia-Pacific Microwave Photonics Conference, TPC Chair of the high-speed and broadband wireless technologies subcommittee of the IEEE Radio Wireless Symposium 2009–2012, TPC Chair of the microwave photonics subcommittee of the IEEE Photonics Society Annual Meeting 2009, TPC Chair of the 2010 IEEE Topical Meeting on Microwave Photonics, General Co-Chair of the 2011 IEEE Topical Meeting on Microwave Photonics, TPC Co-Chair of the 2014 IEEE Topical Meetings on Microwave Photonics, and General Co-Chair of the 2015 and 2017 IEEE Topical Meeting on Microwave Photonics. He has also served as a committee member for a number of international conferences, such as IPC, OFC, BGPP, and MWP. He received the 2005 International Creative Research Award of the University of Ottawa. He received the 2007 George S. Glinski Award for Excellence in Research. In 2008, he received the Natural Sciences and Engineering Research Council of Canada Discovery Accelerator Supplements Award. He was selected to receive an inaugural OSA Outstanding Reviewer Award in 2012 and was one of the top ten reviewers of IEEE/OSA JOURNAL OF LIGHTWAVE TECHNOLOGY 2015–2016. He was an IEEE MTT-S Distinguished Microwave Lecturer for 2013–2015. He received the Award for Excellence in Research 2017–2018 of the University of Ottawa. He is a registered Professional Engineer of Ontario. He is a Fellow of the Optical Society of America and of the Canadian Academy of Engineering.